

Turbulence induced spatial variation of surface temperature in high resolution thermal IR satellite imagery

Lee K. Balick^{*}, Christopher. A. Jeffery^{**}, Bradley Henderson^{***}
Los Alamos National Laboratory, Space and Remote Sensing Sciences Group

ABSTRACT

Atmospheric eddies cause transient spatial and temporal variations of surface temperature and can limit the precision of satellite surface temperature retrievals. If a thermal IR sensor has sufficiently high spatial resolution, the effects of these transient changes of temperature will be seen as variations of the thermal spatial pattern. Nine thermal IR images of a uniform emissivity area on Mauna Loa caldera are carefully compared to document spatial differences between them. These images were obtained from the Dept. of Energy Multispectral Thermal Imager satellite at about 20m GSD. Spatial patterns with a 1C – 6C magnitude are present but not repeated in any of the images. In order to better understand the characteristics and impact of turbulence induced temperature fluctuations for quantitative remote thermal IR sensing, an effort to model the spatial variation of surface temperature as driven by turbulent energy fluxes has been initiated. Stochastic models initially examined showed a close coupling between surface temperature and turbulent fluxes but were not successful. Traditional energy balance models used in this type of simulation are insufficient to model skin temperature because of the importance of the skin layer and its small depth compared to soil depths used in the models. A new treatment based on surface renewal theory is introduced.

1. INTRODUCTION

1.1 Background

Turbulence induced fluctuations of wind speed at the earth surface create temporal variation of surface skin temperatures. Since turbulent eddies move with the prevailing wind, spatial variations of surface temperature result. If the surface response to temperature changes is slower than the atmospheric variations, surface temperature variations are an integrated response to the spatial/temporal structure of turbulence at all scales. Little research relating temporal atmospheric fluctuations to spatial variations of temperature at the surface has been performed. Relevant studies have been performed by Katul et. al.¹ for grass surfaces and Kustas et. al.² for riparian vegetation. It is not uncommon to see the surface temperature variations on fairly uniform surfaces in thermal video images where motion can be used to observe them. However, most satellite thermal imaging sensors have too coarse of a resolution to observe these variations as they average over large areas and, to our knowledge, no one has looked for them. During a field campaign conducted jointly by scientists of the US Department of Energy's Multispectral Thermal Imager³ (MTI) and the U. S. science team for the Advanced Spectral Thermal Emission Spectrometer (ASTER) at the Mauna Loa (Hawaii) caldera, strong evidence of the effects of transient eddies on observed surface temperatures were observed⁴. During this campaign, moving spatial temperature patterns on the scale of 10s of meters were observed with an uncalibrated thermal video system from the caldera rim, radiometric point measurements of surface temperature fluctuated by about 3K over periods of 2 - 3 minutes, and the MTI observed temperature patterns over an area of nearly uniform emissivity. As thermal infrared (IR) remote sensing advances to higher spatial resolution and higher sensor sensitivity, and the need for quantitative measurements of surface temperature develops, spatial variations of 1K and larger over 10's of meters become a significant factor in using and validating these measurements. Relating pixel observations to point or subpixel fluctuations becomes more difficult as does the separation of temperature and emissivity effects.

^{*} lbalick@lanl.gov; phone 1 505 665-1012; fax 1 505 667-3815; <http://www.lanl.gov>; Los Alamos National Laboratory, M/S C323, P. O. Box 1663, Los Alamos, NM 87545 USA

^{**} cjeffery@lanl.gov; phone 1 505 665-9169; fax 1 505 667-3815; <http://www.lanl.gov>; Los Alamos National Laboratory, M/S C323, P. O. Box 1663, Los Alamos, NM 87545 USA

^{***} henders@lanl.gov; phone 1 505 665-2107; fax 1 505 667-3815; <http://www.lanl.gov>; Los Alamos National Laboratory, M/S C323, P. O. Box 1663, Los Alamos, NM 87545 USA

Because turbulence and its effects on surface temperatures are driven by a large set of atmospheric and surface properties, models are needed to study the scope and impact of the relationships between atmospheric conditions and surface temperature variations. It is important to know when this effect will be important for different sensors and how large an effect there will be for retrieving surface temperature with confidence.

1.2 Objectives

This paper presents progress in studies of turbulence induced surface temperature fluctuations in satellite imagery at a site with highly uniform emissivity. Efforts have proceeded in two directions; improved observations over multiple dates, and modeling of the effects of turbulence induced surface temperature variation.

Thermal IR spatial variations will be documented and characterized using multiple MTI images of a portion of the Mauna Loa caldera known to have very small variations of emissivity. Although the study area is not typical of the world, it is excellent for documenting and demonstrating the effects of turbulence induced thermal IR spatial variations because of the highly uniform background at scales of a few meters and larger. These variations will be present over less uniform surfaces but less easy to separate emissivity from other effects.

Initial modeling of the effects of transient turbulent eddies on temporal and spatial variation of surface temperature is presented. Because of the close coupling of the surface skin temperature and wind speed at the molecular boundary interface is so tight, traditional approaches to modeling surface temperature are not successful for this use. Problems have been identified and a new approach to modeling these phenomena are presented. It is the ultimate objective of the modeling effort to develop a capability to examine the magnitude and spatial dimensions of temperature fluctuations for different surfaces in order to evaluate the impact of turbulence induced surface temperature variations on measurements made under different conditions and with different sensors.

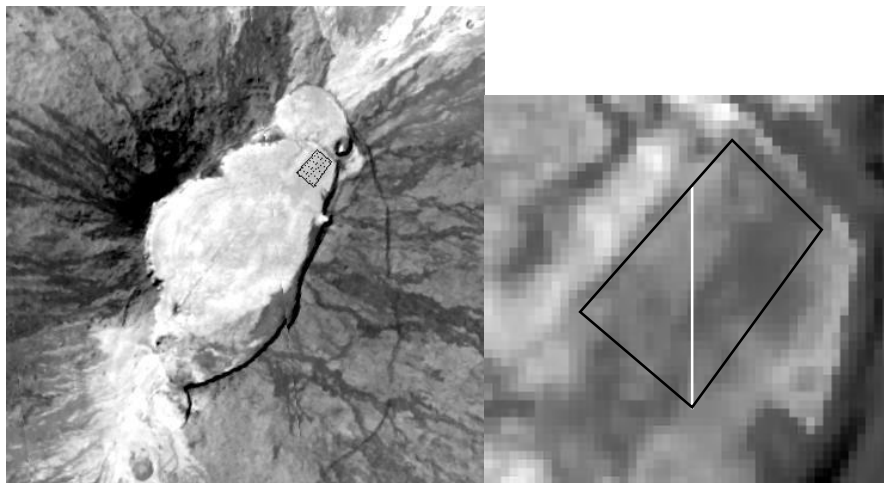


Figure 1. Thermal IR image of the Mauna Loa caldera with the ROI (black) and a zoomed image showing the ROI and the transect used (white).

We present a model that relates surface skin temperature, T_s , and surface-layer air temperature, T_a , for a homogeneous bluff-rough surface. Our model is based on the theory of surface renewal as developed independently by Brutsaert⁵ and Liu and Businger^{6,7}. A key feature of our approach is that molecular diffusion regulates the transport of heat from an adjacent eddy of air into the ground; we extend Brutsaert-Liu-Businger theory by explicitly solving the diffusion equation in molecular sublayers on **both** sides of the air-surface interface. Regulation of surface sensible heat flux by the thin interfacial sublayer located between a turbulent boundary layer and a homogeneous bluff-rough surface was first formulated by Owen and Thomson⁸ and is now well established⁷.

2. METHODS

2.1 Observations

2.1.1 Study Site

The study site is a portion of the Mauna Loa caldera floor at about 4000m above sea level. It has been identified as an area with very high uniformity of surface emissivity with minimum atmosphere effects and a low probability of cloud obscuration. Laboratory measurements of samples show a mean emissivity of 0.970 and a standard deviation of $0.006^{9,10}$. This should not be taken as exact values for imaging because the samples have not been weighted by area. The study area and adjacent surface is a small flow, late in the 1984 eruption of Mauna Loa. No spatial emissivity features have been identified in ground sample measurements or in a previous study by Balick et. al⁴. However, spatial variations of temperature can be caused by unknown subsurface variations. To the extent emissivity effects are constant, image subtraction will remove these features. Figure 1 shows an MTI thermal IR (8.66 μ m) image of the caldera and a zoomed image giving more detail of the study site. The black trapezoid shows the region of interest (ROI) selected for study and the white line shows the location of transects to be shown later.

2.1.2 Image data

The image data used are brightness temperature images of Band M (8.66 μ m) of the MTI satellite. The ground sample distance of the image data is about 20m but the disk containing 85% of the energy from a uniform surface is nearly 32m. The noise equivalent change of temperature is about 0.07K and the system is carefully calibrated. All data are brightness temperature data observed at the top of the atmosphere and are not adjusted for emissivity or atmospheric effects. This study is concerned with spatial variations of temperature and it is assumed that atmospheric effects over the small area are uniform, and Band M is weakly sensitive to atmospheric water vapor.

Nine MTI images of the Mauna Loa caldera are used. The images are co-registered to a precision less than 1 pixel in the area of the ROI. Table 1 gives the MTI image number, date and solar elevation for each image.

Table 1. MTI Images

Image ID Number	Date	Solar Zenith	Cosine Solar Z.
18498	12 June, '00	8.6	0.989
20926	15 July, '00	4.1	0.997
105715	8 Aug. '01	11.5	0.980
106285	1 Sep. '01	14.7	0.967
107309	22 Oct. '01	31.7	0.851
109438	11 Mar. '02	28.8	0.876
109585	22 Mar. '02	25.9	0.900
109602	23 Mar. '02	25.7	0.901
109633	25 Mar. '02	25.3	0.904

A subsection of the nine images is selected for presentation. The subsection contains the study area of the US ASTER Science Team and the vicinity around it. In the following figures, these subsections are individually contrast stretched for visualization of the spatial variation so it is difficult to make quantitative comparisons between them. The region of interest (ROI) has been defined to roughly coincide with the study area of the ASTER science team but adjusted to avoid edge effects. Descriptive statistics, mean, standard deviation, and range, are calculated for the 434 pixels in the ROI. Vertical profiles of brightness temperature extending from the ROI boundary to its southern-most corner are extracted and plotted.

As mentioned, the emissivity and subsurface properties can vary within the study area. To separate these effects from turbulence induced temperature changes, the image with the lowest variability within the ROI (image 109602) was subtracted from the other images. The rationale for this is that the image with the lowest variability is the least effected by turbulence and thus best represents variations in the basalt. Turbulence induced variations will not be the same in any two images and would be preserved. This is, of course, only an approximation: the spatial variations in the difference images cannot be expected to be entirely due to turbulence.

2.2 Model

Models combining thermal remote sensing data and ground-based meteorological data to estimate regional surface sensible heat flux, H , were first developed in the early 1980s¹¹⁻¹³. While the complexity of these models has increased considerably over the last 20 years the underlying principles are unchanged: atmospheric surface layer similarity theory^{14,15} is used to relate H to the bulk properties of the atmospheric surface layer and the difference in temperature between T_a and the aerodynamic temperature of the surface at the effective level of heat exchange, T_0 . As documented in many studies, the most important limitation of thermal remote sensing for the estimation of H arises because T_s is not equivalent to T_0 ^{7,15}.

The difference between T_0 and T_s for a homogeneous bluff-rough surface is controlled by the interfacial sublayer that exists between the surface and the height where the transfer of heat by molecular motion becomes important. Typically this difference is written in terms of an interfacial Stanton number, St ⁷:

$$\langle T_s \rangle - \langle T_0 \rangle = \frac{\langle H \rangle}{u_* \rho_a c_{p,a}} St^{-1} \quad (1)$$

where u_* is the friction velocity, ρ_a is air density, $c_{p,a}$ is specific heat of air at constant pressure, and $\langle \cdot \rangle$ indicates an ensemble average which, in practice, is approximated by a temporal average. Various expressions for St can be found in Table 4.2 of Brutsaert⁷. If T_s is retrieved from remote sensing data then the average skin temperature $\langle T_s \rangle$ in Eq. (1) is replaced by an instantaneous measurement².

2.2.2 Surface renewal theory

In the surface renewal approach⁵⁻⁷, heat transfer in the interfacial sublayer takes place by molecular diffusion into Kolmogorov-size eddies which remain stagnant between the roughness elements for a time, t_* after which they are renewed. Assuming T_s remains constant during stagnation, $T_a(z,t)$ is described by a Green's function solution to the diffusion equation^{5,6}. This solution represents a thermal "wave" that propagates vertically at a speed $(D_a/s)^{1/2}$ where $0 \leq s \leq t_*$ is time since last renewal and D_a is the thermal diffusivity of air. The surface heat flux is:

$$H(s) = -K_a \frac{\partial T_a(z=0, s)}{\partial z} = \frac{K_a}{(\pi D_a s)^{1/2}} (T_s - T_{a,0}) \quad (2)$$

where $T_{a,0}$ is the uniform initial air temperature and $K_a \equiv \rho_a c_{p,a} D_a$ is the thermal conductivity of air. By definition $\langle H \rangle = \int P_s(\zeta) d\zeta H(\zeta)$ where P_s is the probability distribution function of s . Brutsaert⁵ and Liu and Businger⁶ independently assumed $P_s(\zeta) = \langle t_* \rangle^{-1} \exp(-\zeta/\langle t_* \rangle)$ where $\langle t_* \rangle$ is the average renewal rate. Brutsaert⁵ further assumed $\langle t_* \rangle \propto \tau_\eta$ where $\tau_\eta \equiv (\nu z_0 / u_*^3)^{1/2}$ is the Kolmogorov time at the top of the sublayer, ν is the viscosity of air and z_0 is the momentum roughness length. With these assumptions and Eq. (2), Brutsaert⁵ arrived at $St \propto Re^{-1/4} Pr^{-1/2}$ where $Re \equiv u_* z_0 / \nu$ is the roughness Reynolds number and $Pr \equiv \nu / D_a$ is the Prandtl number, in good agreement with experimental data⁷.

2.2.3 A new approach

In Brutsaert-Liu-Businger surface renewal theory discussed in the previous section, T_s remains fixed during an eddy—roughness element heat transfer event. Thus the air temperature is not allowed to "imprint" itself on the surface. Below we derive a new model that links T_a and T_s by considering interfacial sublayers on both sides of the air-surface interface.

Consider a surface renewal event where, as before, $T_a(z,s=0) = T_{a,0}$, but T_s is no longer fixed. Let $T_g(z < 0, t)$ be the ground temperature below the surface-air interface. We assume that the ground is in thermal equilibrium at the beginning of the renewal event, i.e. $T_g(z,s=0) = T_{g,0}$, and that the temperature at the interface is continuous for $s > 0$. Again, the temperature profile, T_p , is given by a Green's function solution to the diffusion equation that is given in Carslaw and Jaeger¹⁶. This solution exhibits a T_s that is constant for $s > 0$ and is given by:

$$T_s(s > 0) = T_{g,0} + \frac{(T_{a,0} - T_{g,0})}{1 + N_{\text{res}}} \quad (3)$$

The key difference between Eq. (3) and the original Brutsaert-Liu-Businger formulation is that T_s is changed by a renewal event. Of principle importance is the new non-dimensional number N_{res} :

$$N_{\text{res}} \equiv (K_g / K_a)(D_a / D_g)^{1/2} \equiv (D_g / D_a)^{1/2}(\rho_g c_{p,g} / \rho_a c_{p,a})$$

where ρ_g is the ground density, $c_{p,g}$ is specific heat of the ground at constant pressure, D_g is the thermal diffusivity of the ground and K_g is the thermal conductivity of the ground. In this work we consider a rock element-air interface with relevant parameters¹³ $K_g \approx 2 \text{ W m}^{-1} \text{ K}^{-1}$, $D_g \approx 8 \times 10^{-7} \text{ m}^2 \text{ s}^{-1}$, $K_a \approx 0.025 \text{ W m}^{-1} \text{ K}^{-1}$, $D_a \approx 2 \times 10^{-5} \text{ m}^2 \text{ s}^{-1}$ giving $N_{\text{res}} \approx 4000$.

The new parameter N_{res} is, therefore, a surface resistance parameter that represents the diffusion-controlled inhibition of $\partial T_s / \partial T_a$ for a given renewal event. The temperature profile, T_p , is shown in Figure 2 for $T_{g,0} = 1$ and $T_{a,0} = 0$. The figure reveals a thermal “wave” that propagates in both the z and $-z$ directions and illustrates the relevant features of Eq. (3): (i) the change in $T_s = T_p(z=0)$ is very small compared to the difference $T_{g,0} - T_{a,0}$ and (ii) the propagation speed is faster in the z direction because $D_a > D_g$.

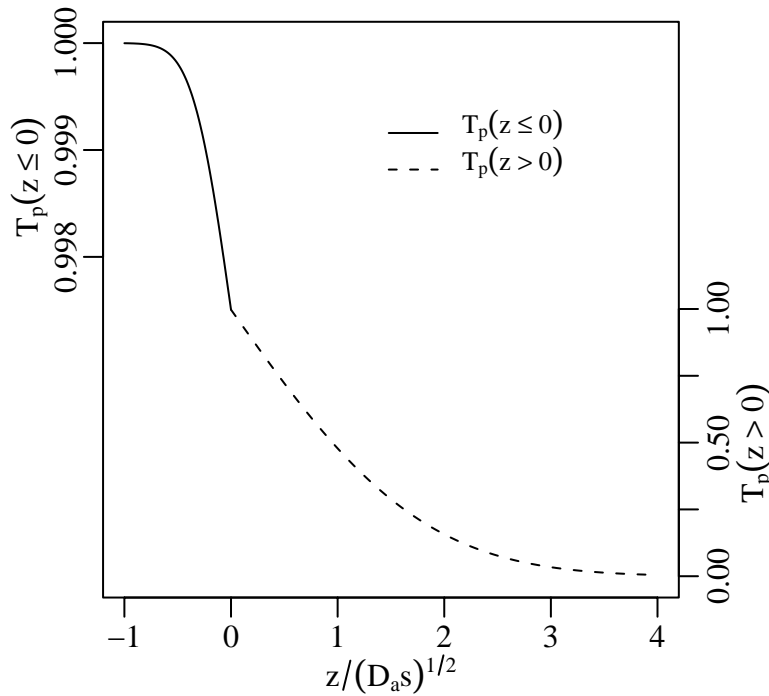


Figure 2. Plot of the Green's function solution for $T_{g,0} = 1$ and $T_{a,0} = 0$.
Other parameter values are given in the text.

From Eq. (3) the change in T_s from an individual renewal event of length t_* is:

$$\Delta T_s = (T_{a,0} - T_s)(1 + N_{\text{res}})^{-1} \quad (4)$$

Technically, this equation does not hold for a subsequent event because the boundary conditions used to derive Eq. (3) no longer hold. On the other hand, $\partial T_p / \partial z$ near $z = 0$ decays as $s^{-1/2}$ and therefore we make the further approximation that Eq. (4) is valid for consecutive renewal events. Averaging over tens of such events and denoting this average with an overbar we find:

$$\frac{d\overline{T_s}}{dt} = \frac{(\overline{T_a} - \overline{T_s})}{\tau_s} \quad (5)$$

where $\tau_s \approx \langle t_*^{-1} \rangle^{-1} (1 + N_{\text{res}})$ and we have implicitly assumed $\overline{t_*^{-1}} = \langle t_*^{-1} \rangle$, i.e. local averages of the rapidly varying renewal time converge to ensemble averages.

Equation (5) is a linear stochastic differential equation with random variable $\overline{T_a}$. If the autocorrelation function of $\overline{T_a}$ has a finite decorrelation then T_s is non-Markovian and its autocorrelation function is non-stationary. In subsequent work we plan to compare the predictions of Eq. (5) with observations.

3. RESULTS AND DISCUSSION

3.1 Observations

The data in Figure 3 show that the variability of surface temperature standard deviation and range as a function of the cosine of the solar zenith angle. It can be seen that temperature variability is invariant over the modest range of solar zenith angles encountered in this data set: 4 to 32 degrees. Figure 4a shows the nine images used in the study but recall that we are characterizing only the area in the ROI shown in Figure 1. Each image was contrast stretched using the ENVI implementation of a gaussian stretch. The earliest image is in the upper left corner with time increasing across the rows and then by row. While none of the images are alike, there are some persistent features inside the ROI and several outside of it. The most prominent feature in the ROI is a dark or low temperature feature running diagonally, upward left to right. This feature might be due to a change of either the surface or the thermophysical properties of the basalt. To try to reduce or minimize the effects of surface or subsurface features, the image with the smallest standard deviation of brightness temperature was subtracted from each of the other images. These are shown in Figure 4b. The dark diagonal feature is reduced or eliminated in many of the images.

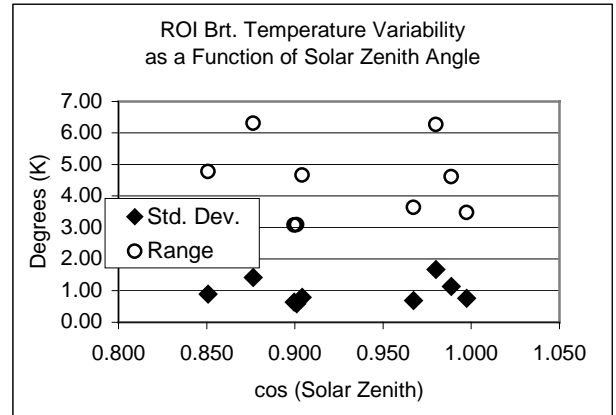


Figure 3. Temperature variability as a function of the cosine of the solar zenith angle.

Figure 5 shows two images of the area at night. To the extent that there is a diagonal feature at night, it is a warm one. This suggests that the daytime cool feature is not due to surface emissivity. It is more likely a change in the thermal properties of the basalt or some other subsurface difference. A cold spot in the last image (lower right image in Figures 3 and 4) is more visible in the difference image and is probably a small cloud. This cold feature has been seen in other transacts (not shown) and several of the images.

Table 2 presents descriptive statistics of brightness temperature in the ROI in both the original and the difference images. The standard deviation of brightness temperature ranges from 0.6K to 1.67 and exceed 1K three of six images. The range of temperature is always greater than 3K, is greater than 4.5K in six of nine images, and greater than 6K in two

images. The variability of the difference images, as measured by these statistics, actually goes up a little on the whole, suggesting that the variability is not strongly tied to emissivity changes. Although the sample of two night images is small, the variability at night seems to be roughly half the magnitude in the day as measured by the standard deviation or range.

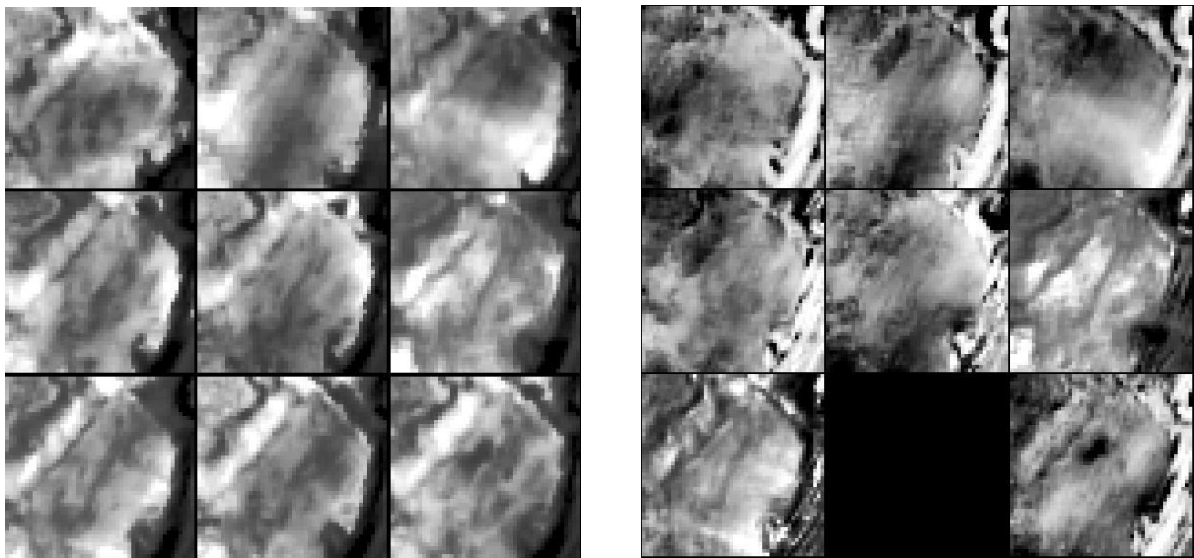


Figure 4. a) Mosaic of the MTI Thermal IR images (8.66μm) and b)a mosaic of the difference images

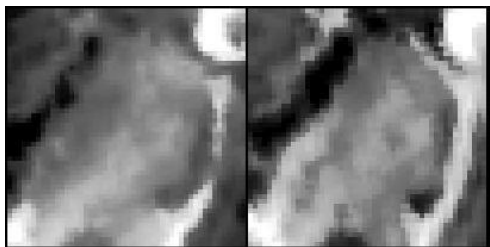


Figure 5. Two night images of the study area.

Table 2. Descriptive statistics or ROI brightness temperature

Image ID	Date	Brightness Temperature (K)			*Differenced Brt. Temp. (K)		
		Mean	Std. Dev.	Range	Mean	Std. Dev.	Range
18498	12-Jun-2000	315.8	1.12	4.6	7.4	1.07	4.3
20926	15-Jul-2000	318.5	0.75	3.5	10.1	0.83	3.9
105715	8-Aug-2001	313.1	1.67	6.3	5.3	1.72	6.8
106284	1-Sep-2001	317.4	0.68	3.6	8.7	0.61	3.3
107309	22-Oct-2001	316.3	0.89	4.8	7.8	1.00	4.6
109438	11-Mar-2002	311.0	1.42	6.3	2.5	1.27	6.0
109585	22-Mar-2002	313.8	0.63	3.1	5.3	0.67	3.2
109602	23-Mar-2002	308.4	0.58	3.1			
109633	25-Mar-2002	297.0	0.78	4.7	-11.7	0.90	5.4
* Image 109602 subtracted from image							

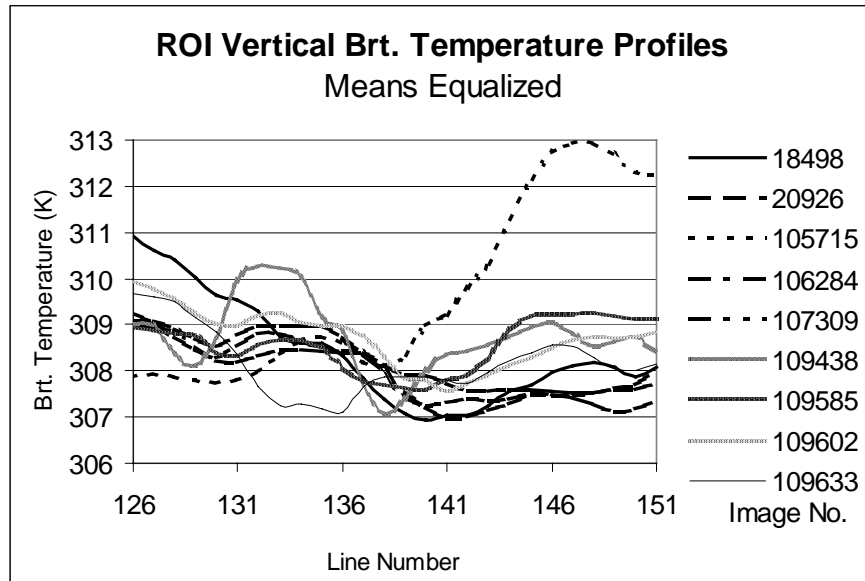


Figure 6. Profiles of brightness temperature through the ROI (means are equalized).

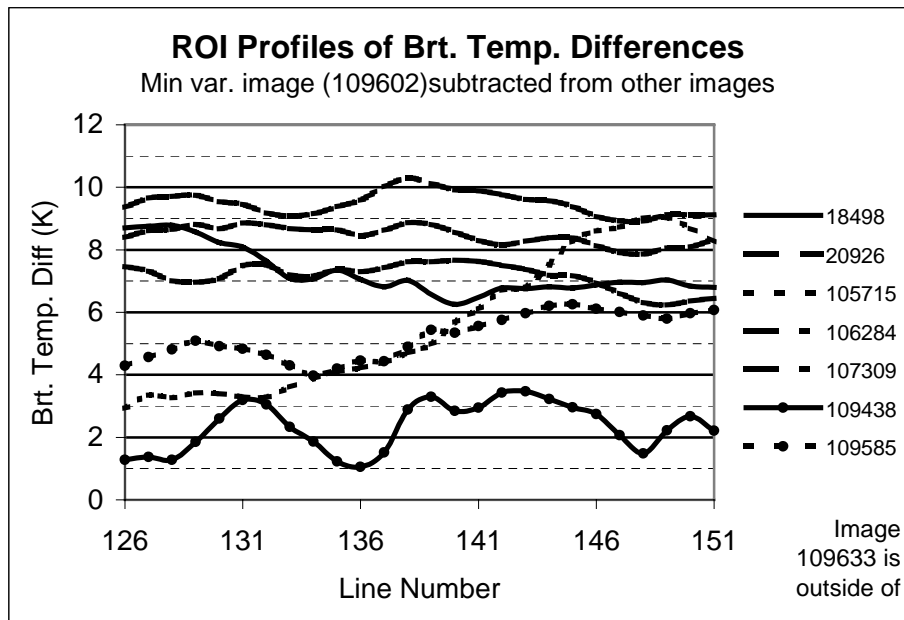


Figure 7. Profiles of temperature difference images through the ROI.

The profile for image 109633 is below $\Delta T=0$ and is not shown.

The profiles of brightness temperature along a vertical line through the ROI (refer to Figure 1) are shown in Figure 6. There are some broad trends present in most, but not all images. In most images there is a downward trend from line 126 at the top of the transect in the image to about line 140, and then temperatures tend to be steady or rise slowly toward the bottom of the ROI. The location of the broad minimum is consistent with the diagonal cool feature seen in most images in Figure 4. Profiles of temperature differences (from image 109602) seem to remove features consistent between images and remove broad trends. This is seen in Figure 7. These plots characterize the transient spatial

variability of brightness temperature reasonably well. Spatially coherent features at different scales with changes on the order of at least 1 – 2K within the transects are common. Since the transect is unlikely to encounter the temperature extremes within the ROI, variations of this magnitude are consistent with the descriptive statistics. On the other hand, the fact that MTI has about 30m samples spaced every 20 m dampens the variability that would be observed by a sensor with higher spatial resolution and sampling.

4. CONCLUSIONS

4.1 Observations

No two thermal IR images of the study area are alike. While there may be some spatially coherent variations of the basalt in the images, they do not explain the spatial variation of brightness temperature within the study area. Difference images are fairly successful at removing the repeatable features. As observed by MTI in its 8.66 μ m channel, the standard deviation of pixel temperature variability is typically over 1K (roughly 0.7 – 1.7K) and the range of temperature in the ROI is about 3 – 6K for. It is probable that the Mauna Loa basalt presents an extreme case for turbulence induced temperature variations with its black rock and very strong insolation. On the other hand, MTI's 30m + pixels may be smoothing the variation considerably (a previous study⁴ indicates a factor of 2 or 3 reduction in standard deviation compared to point measurements). Modern calibrated thermal sensors attempt to achieve temperature measurements with accuracy better than 1K. Since spatial/temporal variations can be larger than 1K, care will have to be taken on the interpretation of pixel retrieval, temperature-emissivity separation, and in correlating ground point measurements with image data. Sensors with higher spatial resolution can be expected to observe higher pixel-to-pixel variations, depending on the surface and the temperature structure.

4.2 Model

A formulation of a new stochastic model relating turbulence to temporal and spatial surface temperature fluctuations has been presented. No model numerical results are available at the time of the writing of this manuscript but initial results will be given at the presentation.

ACKNOWLEDGEMENTS

The observational work was funded by the US National Nuclear Security Administration under contract W-7405-ENG-36 with the Los Alamos National Laboratory, operated by the University of California. Drs. Donald Sabol and Alan Gillespie at the W. M. Keck Remote Sensing Laboratory at the University of Washington, as well as Drs. Elsa Abbott and Anne Kahle at the NASA Jet Propulsion Laboratory, have provided data, photographs, and many valuable discussions which have enabled this work. We have not listed them as coauthors but the observational characterization of temperature variability is one component of a larger group effort. Scientists from the Savannah River Technology Center performed the early ground measurements that initially characterized the spatial-temporal variations at the caldera.

REFERENCES

1. G. G. Katul, J. Schieldge, C. Hsieh, and B. Vidacovic, "Skin temperature perturbations induced by surface air turbulence over a grass surface", *Water Resour. Res.*, Vol. 11, No. 5, pp 1265-1274, 1998.
2. W. P. Kustas, J. H. Prueger, and L. E. Hipps, "Impact of using different time-averaged inputs for estimating sensible heat flux of riparian vegetation using radiometric surface temperature" *J. Appl. Meteorology*, Vol. 41, pp. 319-331. 2002.

3. J. J. Szymanski, W. H. Atkins, L. K. Balick, C. C. Borel, W. C. Clodius, W. R. Christensen, A. B. Davis, J. C. Echohawk, A. E. Galbraith, K. L. Hirsch, J. B. Krone, C. K. Little, P. M. McLachlin, A. M. Morrison, C. Novak, K. Pollock, K. Ramsey, E. E. Riddle, C. A. Rohde, D. C. Roussel-Dupre, B. W., Smith, K. Smith, K. Starkovich, J. P. Theiler, and P. G. Weber, "MTI science, data products, and ground-data processing overview. *Proc. of SPIE*, Vol. 4381, Orlando FL, 16-19 April, 2001. pp 195-203. 2001.
4. L. K. Balick, A. R. Gillespie, E. Abbott, D. Sabol, A. B. Kahle, C. C. Borel, and M. Pendergast, "Multiscale thermal-infrared measurements of the Mauna Loa caldera, Hawai'i", *Proc. of SPIE*, Volume 4381, Orlando FL. pp 440-446, 2001.
5. W. Brutseart, "A theory for local evaporation (or heat transfer) from rough and smooth surfaces at ground level". *Water Resour. Res.*, Vol. 11, No. 4, pp 543-550, 1975.
6. W. T. Liu and J. A. Businger, "Temperature profile in the molecular sublayer near the interface of a fluid in turbulent motion", *Geophys. Res. Let.*, Vol. 2, No. 9, pp 403-404, 1975.
7. W. Brutseart, *Evaporation into the Atmosphere*, D Reidel Pub. Co., Dordrecht, Holland, 1982.
8. P. R. Owen and W. R. Thomson, "Heat transfer across rough surfaces", *J. Fluid Mech.*, Vol. 15, pp321-334, 1963.
9. D. Sabol, Personal communication, W. M. Keck Remote Sensing Laboratory, University of Washington, Seattle WA USA. 2002.
10. E. Abbott, Personal communication, NASA Jet Propulsion Laboratory, Pasadena CA USA. 2002.
11. G. J. R. Soer, "Estimation of regional evapotranspiration and soil moisture conditions using remotely sensed crop surface temperatures", *Remote Sens. Environ.*, Vol. 9, pp 27-45, 1980.
12. J. C. Price, "The potential of remotely sensed thermal infrared data to infer surface soil moisture and evaporation", *Water Resour. Res.* Vol. 16, No. 4, pp 787-795, 1980.
13. L. K. Balick, R. K. Scoggins and L. E. Link. "Inclusion of a simple vegetation layer in terrain temperature models for thermal IR signature prediction. *IEEE Trans. Geosci. Remote Sens.*, Vol. GE-25, No. 3, pp 143-152, 1981.
14. A. S. Monin and A. M. Obukhov, "Basic laws of turbulent mixing in the ground layer of the atmosphere", *Tr. Geofiz. Inst. Akad. Nauk SSSR*, Vol. 24, pp 163-187, 1954.
15. R. B. Stull, *An Introduction to Boundary Layer Meteorology*. Kluwer Academic Publishers, Holland, 1988.
16. H. S. Carslaw and J. C. Jaeger. *Conduction of Heat in Solids*, 2nd. Edition, Oxford University Press, Oxford, United Kingdom, 1959.